Arabian Journal for Science and Engineering (2022) 47:7147–7155
https://doi.org/10.1007/s13369-022-06725-5

RESEARCH ARTICLE-CHEMISTRY

The Carbon-Based 3D-Hierarchical Cathode Architecture for Li-Ion Batteries

Aslan Coban[1] · **Hatice Gungor**[2]

Received: 6 July 2021 / Accepted: 17 February 2022 / Published online: 12 March 2022

Abstract

High-purity NMC111 nanoparticles are obtained by sol–gel synthesis. NMC111/MWCNTs freestanding hybrid composite cathodes are produced by a simple vacuum filtration process without detriment to both the crystalline and morphologic structures of the NMC111 nanoparticles. NMC111/MWCNTs freestanding hybrid composite cathode materials exhibit enhanced cycling stability, long cycle life, and high specific discharge capacity compared with pure NMC111 electrode, which is prepared by the classic slurry method. After 1000 cycles, within 2.5–4.6 V working potential range (at 1 C-rate), the specific discharge capacity of NMC111/MWCNTs freestanding hybrid composite cathode is 118.5 mAh g^{-1} with a capacity loss rate of 44.2%, considerably higher than the result of pure NMC111 cathode electrode (84.9 mAh g^{-1} with a capacity loss rate of 59.2%). NMC111/MWCNTs freestanding hybrid cathode has shown lower polarization and good cyclic stability when compared with the pristine NMC111 cathode electrode in the cyclic voltammetry (CV) analysis. MWCNTs in the electrode have high electron conductivity and easies the electron transfer during the electrochemical charge/discharge. Graphite@NMC111/MWCNTs full cells were fabricated to support results acquired with the half cells. To analyze the working of MWCNTs-reinforced freestanding composite cathode in full cell, graphite@NMC111/MWCNTs combination was constituted and obtained a specific discharge capacity of 150.7 mAh g^{-1} with a capacity loss of 30.4% after 1000 cycles. Extreme cycling and structural stability increased conductivity, and a high cycle number is reached by compressing the NMC111 nanoparticles between MWCNTs. Highly electrical conductive MWCNTs, which are homogeneously dispersed on around the NMC111 nanoparticles, are employed as both structural strengthening components and surface improvers for NMC111 cathode electrodes, not only for enhancing the electrical conductivity but also supplying powerful guarding to the side reactions with the liquid electrolyte. The results have shown that the MWCNTs-based freestanding electrode form can be widely used electrode type for high-level featured lithium-ion batteries.

Keywords NMC111 ($LiNi_{0.33}Mn_{0.33}Co_{0.33}O_2$) · MWCNTs (multi-wall carbon nanotubes) · Freestanding · Cathode · Li-ion battery

1 Introduction

In recent times, the use of Li-ion batteries as a power source for electric vehicles (EVs) has become widespread [1]. In order to stand out in the battery market, more performance improvements should be made to achieve a longer driving range of EVs, and there should be a significant reduction in costs [2, 3]. The realization of this target largely depends on the cathode active material; among the potential cathode materials, layered $LiNi_xMn_yCo_zO_2$ ($x + y + z = 1$), lithium nickel manganese cobalt (NMC) oxide, is one of the most attractive cathode materials [4]. NMC cathode materials are the common solid composition of $LiNiO_2$, $LiMn_2O_4$, and $LiCoO_2$, which are crystallized in a structure similar to α-$NaFeO_2$ in the R^{-3} m space group [5]. Ni component advances the reversible capacity, Co component reduces cation mixing, and Mn component increases structural stability; thus, NMC is the most popular cathode materials [6]. This

✉ Aslan Coban
acoban@subu.edu.tr

Hatice Gungor
g.hatice.19@hotmail.com

[1] Department of Mechanical Engineering, Technology Faculty, Sakarya University of Applied Sciences, Esentepe Campus, 54187 Sakarya, Turkey

[2] Research, Development and Application Center, Sakarya University, 54187 Sakarya, Turkey

cathode material has a layered structure in which Li^+ ions deposited in between the consecutive layers of edge-shared MO_6 octahedra. In this layered structure, the electrochemical transport of Li^+ ions happens by oxidation/reduction of Ni^{2+}/Ni^{4+} and Co^{3+}/Co^{4+} ions [7]. However, Mn^{4+} ions are inactive and Mn stabilizes the host structure during Li^+ ions input/output. $LiNi_{0.33}Co_{0.33}Mn_{0.33}O_2$ (NMC111) exhibited a specific capacity 160 mAh g^{-1} between 2.5 and 4.3 V and 200 mAh g^{-1} between 2.8 and 4.6 V [7, 8]. Its layered structure with changing volume less than 2% provides high specific capacity and good stability during Li^+ insertion/extraction [9–11]. However, lithium transition metal oxides, such as NMC, show nominal electrical conductivity between 10^{-7} and 10^{-2} S cm^{-1} in different states of charge. Polymer binders, which are generally electrically insulating, reduce electronic conductivity, even more, when mixed with other substances [12]. Electronic transmission is the speed-limiting parameter for power performance at cathodes without conductive reinforcement. To increase electronic conductivity, conductive additives (usually carbon black) are used in cathode production. Particularly, constituents of the electrolyte are responsive to high temperatures [13].

Carbon black particles (0D) generate electronic paths owing to the point-to-point contact between them and the effective substance particles in the electrodes. For this reason, great amounts of carbon black are used in the electrode composition to arrive desired electrical conductivity. Large amounts of conductive carbon black are required during electrode production to obtain the expected electronic conductivity from the electrode [12]. One-dimensional CNTs from other conductive additives are researched by many researchers to improve both electrochemical and structural properties of cathode electrodes [14]. MWCNTs' "line-to-line" touch with others and "line-to-point" touch with effective material grains constitute three-dimensional (3D) conductive networks in the internal structure of the electrode [15, 16]. Du et al. NMC532 observed that when CNTs were supplemented to the cathode electrode, the cycle performance was improved by approximately 99.4% capacity retention after 200 cycles. They also reported that CNTs supplement reduced battery cost [17, 18].

Recently, the improvement of high energy density, high discharge capacity long cycle life performance, light and binder-free electrodes for Li-ion battery systems used in more light electric/hybrid vehicles and portable electronic appliances have been expedited. Recently reported studies have been declared as light, high discharge capacity, long cycle life, and binder-free, flexible freestanding electrodes for seconder battery systems [19, 20]. Additionally, in electrolyte solution of commercial LIBs, even though the amount of the water in $LiPF_6$ salt is negligible, it accelerates the corruption of the $LiPF_6$ salt at higher temperatures than 40 °C and at elevated potentials (> 4 V vs. Li/Li^+). HF has consisted as a by-product during the decomposition of the salt, thus, the $LiPF_6$ salt decomposes non-stop. Although solutions containing $LiPF_6$ salt passivated under alkyl carbonate, metallic current collectors corrode, because of their reaction with HF throughout the lifetime of the battery [21].

In this study, the generation, and electrochemical effects are reported based on a 3D electronic conductive network by MWCNTs in the freestanding cathode electrode production of NMC111. Sub-micron particles, the fast, basic, and low-cost sol–gel are preferred for producing NMC111. In the freestanding electrode, produced NMC111 particles have domiciled between MWCNTs by vacuum filtration method to evolve cathode conductivity and rate performance. The influences of the MWCNTs on the electrochemical performance of the both coin cell and full cell are explored. The electrochemical performances of the NMC111 classic electrode, and NMC111/MWCNTs freestanding hybrid composite cathode electrodes in the half cell, and full cell formed with NMC111/MWCNTs freestanding cathode and a graphite anode have been examined along 1500 cycles, at 2.5–4.6 V.

2 Experimental Works

The following different successive stages are explained for the achievement of the procedure in this work.

2.1 Synthesis of NMC111 Particles

NMC1111 particles were synthesized via sol–gel (Fig. 1). In this process, 1 M Li-nitrate ($(CH_3COO)0.2H_2O$), Ni-acetate ($Ni(CH_3COO)_2{\cdot}4H_2O$), Mn-acetate ($C_4H_6MnO_4{\cdot}4H_2O{\cdot}C_4$), Co-acetate ($C_4H_6CoO_4{\cdot}4H_2O$) (0.33:0.33:0.33) were employed as beginning materials, and citric acid ($C_6H_8O_7$) was also utilized as a gelling agent. Beginning materials and citric acid were dispersed in 100 ml bidistilled water and stirring has proceeded until a clear viscous gel was formed at 90 °C. The gel is dried for 24 h at 85 °C and then calcined at 400 °C for 3 h and 900 °C for 12 h in the air.

2.2 Electrode Fabrication

In this study, pristine NMC111 cathode and graphite anode were prepared by the classic slurry preparation method, while NMC111/MWCNTs freestanding electrodes were prepared by vacuum filtration method. In the classic slurry preparation method, a slurry containing active particles (90 wt%), carbon black (5 wt%), and PvDF binder (5 wt%) dissolved in an *N*-methyl-2-pyrrolidinone solution (NMP). The final anode and cathode slurries were then coated onto the thin copper foils

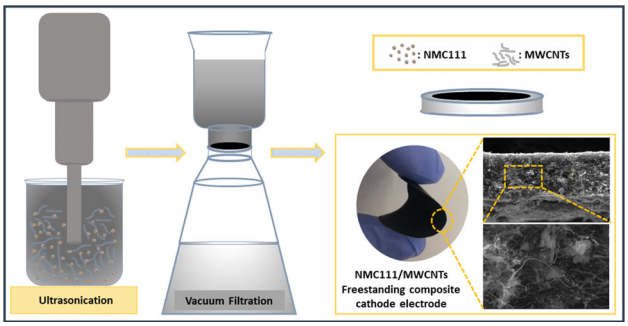

Fig. 1 The preparation process of NMC111/MWCNTs freestanding composite cathode electrode

(thickness 18 μm, MTI, USA) and aluminum foils (10 μm, MTI, USA) by Doctor Blade.

In freestanding cathode electrode preparation, 25 mg NMC111 cathode active particles, 50 mg MWCNTs, 60 mg SDS (sodium dodecyl sulfate) (Sigma-Aldrich), and PVA (Polyvinyl alcohol) (Sigma-Aldrich) was added in 50 mL bidistilled water and sonicated for 40 min. The mixing then was vacuum-filtered by depositing on filter paper. The deposited electrode material was peeled-off from paper and dried in a vacuum at 60 °C (see Fig. 1). The NMC111 loading of tested classic electrode was 8.12 mg_{NMC111}/cm^2 with an electrode thickness of ≈ 110 μm. For the freestanding electrode, NMC loading of the freestanding cathode electrode was 7.21 mg_{NMC111}/cm^2 with an electrode thickness of ≈ 50 μm. The copper foil was used as a current collector (10 μm, MTI, USA) from which electrodes with a diameter of 9 mm diameter were cut. For graphite@NMC111 cells, the graphite amount was 7.1 $mg_{graphite}/cm^2$ (thickness of ≈ 90 μm).

2.3 Materials Characterization

The shape and size of the NMC111 nanoparticles and section morphology of NMC111/MWCNT were examined using a field emission scanning electron microscope (FE-SEM, FEI Quanta Q400). The phase compositions and crystallinity of the NMC111 nanoparticles and NMC111/MWCNTs freestanding electrodes were controlled by X-ray diffraction technique (XRD, Rigaku DMax 2200) using a diffractometer equipped with a Cu anticathode ($K\alpha_{1,2}$). Raman spectra were collected using a Kaiser RXN1 instrument. The laser wavelength was 785 nm in this study.

2.4 Electrochemical Characterization

Electrochemical tests were applied on a CR2032 coin type cell, assembled in an argon-filled glove box, produced NMC111 and NMC111/MWCNTs as the working electrode, lithium metal as the opposite electrode, 1 M $LiPF_6$ solution (Sigma-Aldrich, battery grade) as the electrolyte, and polypropylene membrane (Celgard 2400) as the separator. Galvanostatic charge/discharge tests were performed between 2.5 and 4.6 V (vs. Li/Li^+), at 1C (0.3 mA/cm^2) state of charge conditions (1C = 279 mAh g^{-1}) at room temperature. Cyclic voltammetry (CV) was performed between 2.4 and 4.6 V (vs. Li/Li^+) at a scan rate of 0.25 mV/s. The electrochemical impedance spectrum (EIS) was tested in a frequency range from 100 kHz to 0.01 Hz.

3 Results and Discussion

Figure 2 shows the XRD patterns of cathode materials NMC111 powders and NMC111/MWCNTs freestanding electrode. A layered structure based on a hexagonal α-$NaFeO_2$ structure with R3m space group is observed for NMC111 powders without any obvious impurities and secondary phases [28]. Lattice parameters of NMC111 powders were calculated as $a = 2.861$ Å and $c = 14.153$ Å by least squares method and the results are presented in Table 1. The *c/a* ratio is defined as the lattice distortion and this ratio is 4.947 in our work.

The increase in the c/a ratio indicates that the distortion in the crystal lattice structure is reduced [8]. The split peaks of (006)/(102) and (108)/(110) are difficult to separate from each other, suggesting a more developed crystalline layered structure [18]. The R-factor $((I_{(006)} + I_{(012)})/I_{(101)})$ of the NMC111 powders was calculated as 0.437, which is less than previous studies. The lower *R*-value indicates a better hexagonal layered structure [27]. Moreover, $I_{(003)}/I_{(104)}$ intensity ratio of all samples demonstrated cation mixing (Li^+/Ni^{2+}) [29]. In previous investigations, the ratio $I_{(003)}/I_{(104)}$ is less than 1.33, and hence, they are expressed that unwanted cation mixture existed in structure [25, 26], whereas in our study the $I_{(003)}/I_{(104)}$ intensity ratio is 1.653. This ratio clearly shows that there is no cation mixture in the structure. Pure NMC111 powders and NMC111/MWCNTs freestanding hybrid electrodes have both high purity, regular and sturdy layered structures. In the XRD pattern of the hybrid electrodes, peaks at around 26° are attributed to the (002) of the MWCNTs [30].

Raman spectroscopies of the NMC111 and NMC111/MWCNTs freestanding electrodes are shown in Fig. 3. Raman spectra of NMC111 and NMC111/MWCNTs freestanding electrodes before cycling were measured in the air within ~ 1 h with the samples not treated prior to measurements.

The bands in Raman spectra; (i) the vibrational features of NMC111 with Ni–O mode at 471 cm^{-1} and the broadband at 599 cm^{-1} are attributed to the Co–O/Mn–O stretching modes; (ii) two broad Raman bands of the carbon caused by MWCNTs are associated with the D-band, G-band, and 2D-band at 1380, 1589 and 2700 cm^{-1}, respectively. The

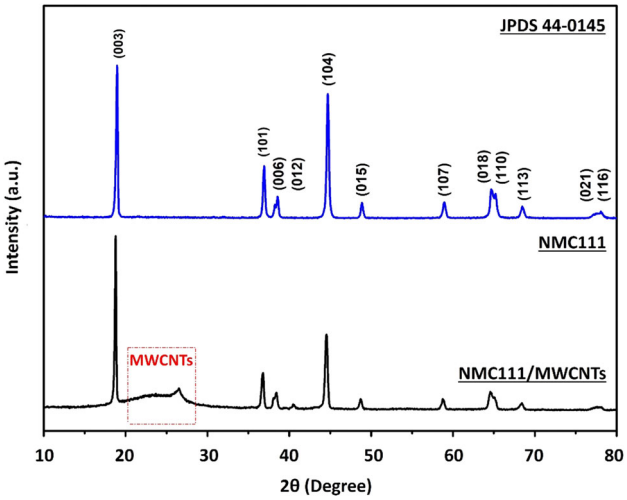

Fig. 2 XRD patterns of the pristine NMC11 powders and NMC111/MWCNTs freestanding hybrid electrodes

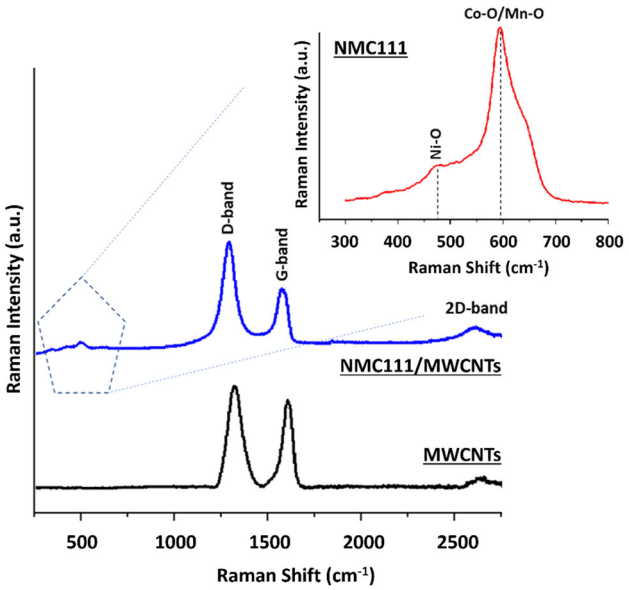

Fig. 3 Raman spectra of the pristine NMC111 powders and NMC111/MWCNTs freestanding hybrid electrode

Table 1 The lattice parameters of pristine NMC111 powders

Lattice parameters	NMC111	The lattice parameters of NMC111 in the literature	
a (Å)	2861	~ 2864	[22–24]
c (Å)	14,153	~ 14,247	[22–24]
c/a	4947	4976	[8, 22–24]
$I_{(003)}/I_{(104)}$	1.653	> 1.33	[25, 26]
$R\ ((I_{(006)} + I_{(012)})/I_{(101)})$	0.437	~ 0.45	[27]

D-band (disordered carbon band) is defined as a double resonance peak generated by the fault or irregularity in the carbon sequencing and the G-band (graphitic band) arises from the in-plane vibration of sp^2 carbon atoms [31]. D and G-bands have high intensity owing to the powerful Raman scattering of carbon.

Figure 4 shows FE-SEM images of as-synthesized NMC111 particles, pure NMC111 electrode, and NMC111/MWCNTs freestanding electrode at various magnifications. From Fig. 4a, NMC111 particles have a polyhedral form, and the sizes of particles are between 80 and 150 nm. Figure 4b, b1 presents that NMC111 particles agglomerated, because of PVDF binder when classic slurry preparation. PVDF ensures enough adhesion between the NMC111 particles and between the electrode components and the Al foil.

Figure 4c, c1, and c2 indicates cross section images of NMC111/MWCNTs freestanding electrodes at various magnifications. These images express that MWCNTs wrap NMC111 particles and thus prevent to agglomeration of uniformly distributed NMC111 particles. MWCNTs not only serve as a conductive agent, but also keep together NMC111 nanoparticles like a binder. In addition, the conductive MWCNTs act as a structural skeleton supporting the electrode totality and provide a developed porous structure. Thus, a binder and current collector-free electrode preparation become possible and this process does not contain dangerous solvents [32, 33]. Figure 4d shows that the energy-dispersive X-ray spectroscopy method has analyzed the chemical composition distribution images of NMC111/MWCNTs. NMC111 particles are homogeneously decorated between the conductive network of MWCNTs throughout the cross-sectional area.

The electrochemical performance of NMC111 and NMC111/MWCNTs cathode electrodes are analyzed in the potential range of 2.5–4.6 V (vs. Li/Li^+) with a scan rate of 0.25 mV/s by cycle voltammetry (CV). NMC111 and NMC111/MWCNTs cathodes are working electrodes, metallic Li is counter and reference electrode. In Fig. 5a, CV curve of NMC111, only one couple of wide peaks are suitable to the redox reactions of Ni^{2+}/Ni^{+4}. The peaks at ∼ 3.85 V and 3.63 V are connected to the anodic/cathodic reaction of Ni^{2+}/Ni^{+4} [34]. Shaju et al. expressed that the Ni^{2+}/Ni^{4+} redox reactions happened in 3.7–3.9 V, while for Co^{3+}/Co^{4+} anodic reaction was executed about at 4.5 V and also Mn^{4+} ions did not join in redox reaction in this voltage window [35]. Hong et al. informed that the oxidation of Ni occurred in two steps: first step $Ni^{2+} \rightarrow Ni^{3+}$ at 3.7–3.9 V, the second step is $Ni^{3+} \rightarrow Ni^{4+}$ at 3.9–4.4 V. That's why the reaction of Ni during charging/discharging is accepted as oxidation of $Ni^{2+} \rightarrow Ni^{4+}$ [34]. CV curves of the NMC111/MWCNTs composite cathode electrode are shown in Fig. 5b. The polarization of each cycle does not have clear differences between the anodic

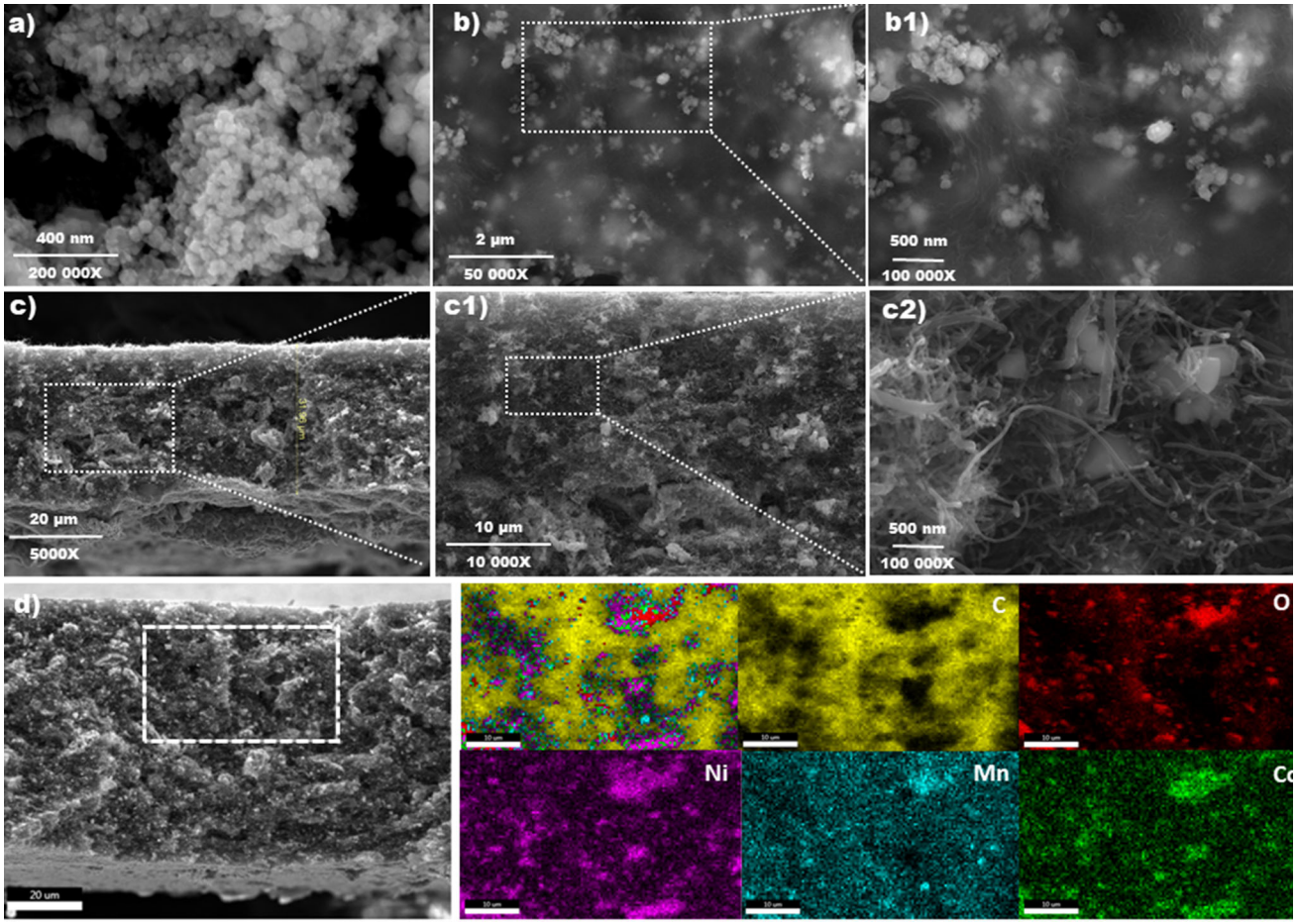

Fig. 4 FE-SEM images of (**a**) pristine NMC111 powders, (**b**) NMC111 electrode produced by traditional method, (**b1**) FE-SEM image of NMC111 electrode produced by traditional method at higher magnification, (**c**) cross section of NMC111/MWCNTs freestanding hybrid electrode, (**c1**, **c2**) FE-SEM images of NMC111/MWCNTs freestanding hybrid electrode at higher magnification and (**d**) EDS dot-mapping images of NMC111/MWCNTs freestanding hybrid electrode

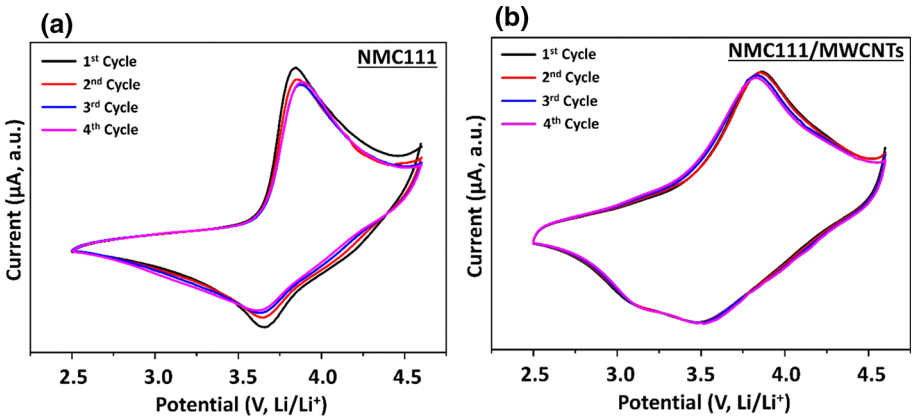

Fig. 5 Cycle voltammetry curves of the (**a**) NMC111 electrode and (**b**) NMC/MWCNTs freestanding hybrid electrode

and the cathodic reaction peaks at around 3.5 V and 3.82 V. The cathodic peak around 3.0 V explains reduction peak of Mn^{4+} to Mn. The exactly oxidized Mn^{4+} ions stabilize the lattice structure due to inactive [22]. NMC111/MWCNTs freestanding cathode and shown lower polarization and good cyclic stability when compared with the pristine NMC111 cathode electrode. MWCNTs in the electrode have high electron conductivity and easies the electron transfer during the electrochemical charge/discharge [36].

The electrochemical performance of NMC111/MWCNTs freestanding cathode electrode was controlled by used in both half cell and full cell. Figure 6a presents the galvanostatic charge–discharge results of the NMC111 electrode, NMC111/MWCNTs freestanding electrode, and NMC111/MWCNTs@Graphite full cell which indicate typical properties of an NMC111-based composite cathode in between 2.5 and 4.6 V at 1C-rate. Galvanostatic charge–discharge results of cathodes demonstrate a characteristic working potential of NMC111 at around 3.7 V.

In Fig. 6a, b, NMC111 cathodes electrode exhibits 208 mAh g^{-1}, 154.6 mAh g^{-1}, and 84.9 mAh g^{-1} at first cycle, 500th cycle, and 1000th cycle. NMC111/MWCNTs composite freestanding electrode demonstrates 212 mAh g^{-1}, 180.8 mAh g^{-1}, and 118.5 mAh g^{-1} at first cycle, 500th cycle, and 1000th cycle. At the end of 1000th cycle, the discharge capacity of NMC111/MWCNTs freestanding electrode is higher than discharge capacity of NMC111 electrode due to the addition of the MWCNTs with superior conductivity. The nested cylindrical conductive channels of MWCNTs have reduced the polarization, because of eased electron transfer during the charge–discharge process. The larger specific area of the MWCNTs provides more ways for the Li^+ transfer between the cathode and electrolyte [12]. At the same time, MWCNTs serve as an electronic conducting binder by replacing conventionally used carbon black and polymeric binders in the freestanding electrode [37]. Figure 6c shows electrochemical performance results of graphite @NMC111/MWCNTs full cell, which 216.5 mAh g^{-1}, 177.3 mAh g^{-1}, and 150,7 mAh g^{-1} at the first cycle, 500th cycle, and 1000th cycle, respectively. The discharge capacity of NMC111/MWCNTs@graphite full cell is lower than the discharge capacity of NMC111/MWCNTs half cell after 500 cycles. The causes of this reduction in capacity are likely formation of CEI (cathode electrolyte interphase), electrolyte oxidation, and the formation of the SEI (solid electrolyte interphase) which is composed in the first cycles [38]. In Fig. 6d, NMC111, NMC111/MWCNTs half cells, and graphite@NMC111/MWCNTs full cell gives capacity loss of 59.2%, 44.2%, and 30.4% vs. to the initial specific discharge capacity, after 1000 cycles. The results compared in Table 2 approved that freestanding electrodes reinforced with MWCNTs improved the electrochemical performance of Li-ion batteries because of the 3D porous and flexible structure.

The smaller NMC111 particle size and the conductivity of the MWCNTs facilitated the electron/ion transfer during the anodic–cathodic reactions because they prevented Li^+/Ni^+ mixing [22, 39]. Owing to, large surface area, the high conductive and 3D porous structure of MWCNTs supply more transfer paths for the Li^+ ion diffusion between the cathode and electrolyte, decreasing the polarization [40, 41].

Also, the electrochemical resistance of NMC111 cathode, NMC111/MWCNTs freestanding composite electrode, and graphite@NMC111/MWCNTs full cell is examined using electrochemical impedance spectroscopy in Fig. 7. The semicircles represent the SEI impedance and the diameter of the semicircles defines charge transfer impedance at the electrode and electrolyte interface.

The sloping line indicates Warburg impedance which diffusion resistance of Li^+ in the electrode. Nyquist plots are fitted to an equivalent circuit and shown in Fig. 7. In the equivalent circuit, R_e symbolizes the electrolyte resistance and R_{sf} and CPE_{sf} symbolize resistances and capacitances of SEI film R_{ct} and CPE_{ct} symbolize resistances and capacitances of the interface, respectively, and W symbolizes Warburg impedance [42]. The charge transfer resistances of NMC111, NMC111/MWCNTs, and graphite@NMC111/MWCNTs are obtained 61 Ω, 29 Ω, and 37 Ω, respectively. The charge transfer resistance of cells is significantly improved with the addition of MWCNTs. The electronic and ionic transfer have speeded up and charge transfer resistance has decreased, because of the MWCNTs added to NMC111 [43]. Also, MWCNTs have improved the electrochemical performance of graphite@NMC111/MWCNTs full cells.

In addition, the lithium-ion diffusion coefficient was further calculated according to Eq. (1), where D is the lithium-ion diffusion coefficient, σ_w is the slope of Warburg curve, R is the gas constant (8.314 J mol^{-1} K^{-1}), T is the absolute temperature (298.15 °K), A is the electrode area, n is the number of electrons transferred per molecule during the electrochemical reaction, F is Faraday constant (96,485.33 C mol^{-1}), and c is the molar concentration of Li^+ and accepted as 1 mol L^{-1} [42].

$$D = R^2T^2/2A^2n^4F^4c^2\sigma_w^2. \quad (1)$$

By using this equation, the lithium-ion diffusion coefficients of the NCM111, NMC111/MWCNTs, and graphite@NMC111/MWCNTs ARE calculated as 1.04 × 10^{-10} cm^2 s^{-1}, 7.62 × 10^{-11} cm^2 s^{-1}, 7.07 × 10^{-11} cm^2 s^{-1} and 3.89 × 10^{-11} cm^2 s^{-1}, respectively (Table 3). NMC111/MWCNTs half cell displays the highest lithium-ion diffusion coefficient, which proves that the 3D electronic conductive network formed by MWCNTs is convenient

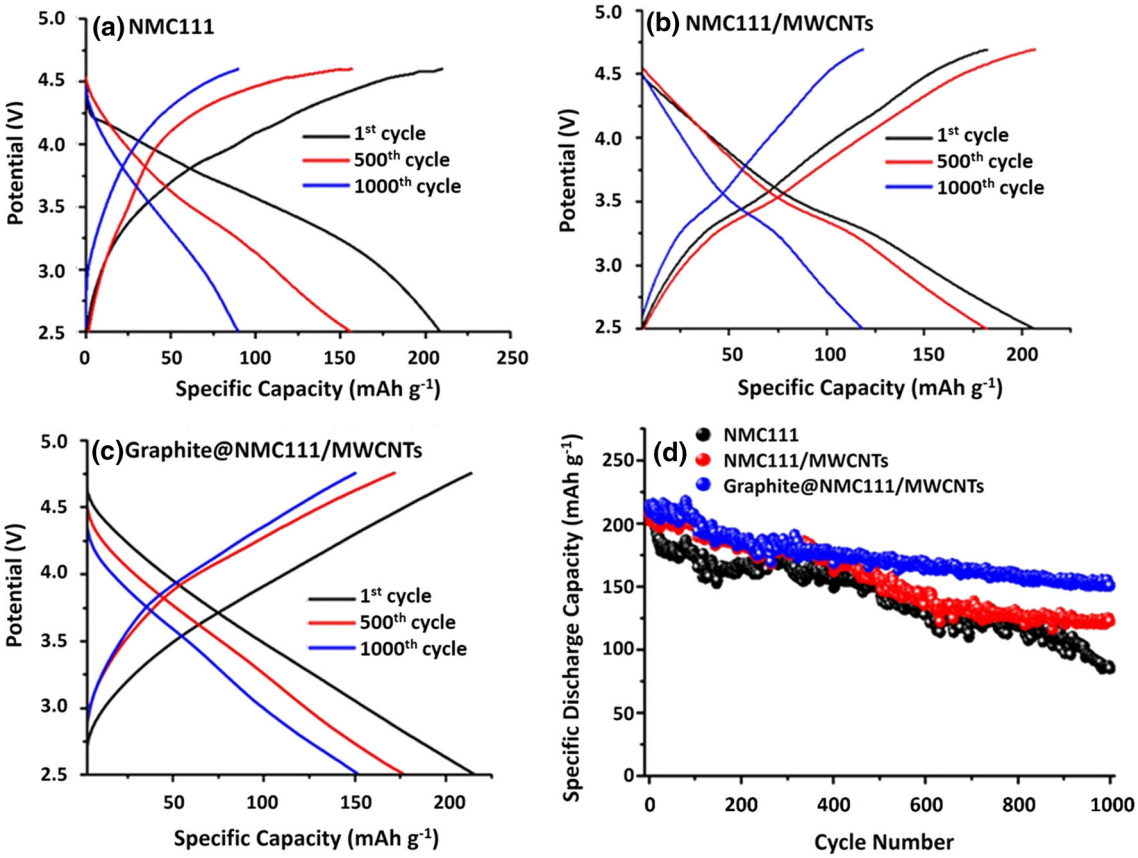

Fig. 6 Galvanostatic charge/discharge tests of (**a**) NMC111 electrode, (**b**) NMC111/MWCNTs half cell, (**c**) graphite @NMC111/MWCNTs full cell, and (**d**) cycle number specific discharge capacities of NMC111 (black), NMC111/MWCNTs half cell (red), and graphite @NMC111/MWCNTs full cell (blue)

Table 2 Specific discharge capacity values and capacity loss ratios of NMC111, NMC111/MWCNTs, and graphite@NMC111/MWCNTs

Electrode	Initial capacity (mAh g^{-1})	After 500th cycle, specific discharge capacity (mAh g^{-1})	After 1000th cycle, specific discharge capacity (mAh g^{-1})	Capacity loss ratio (%)
NMC111	208	154.6	84.9	59.2
NMC111/MWCNTs	212	180.8	118.5	44.2
Graphite@NMC111/MWCNTs	216.5	177.3	150.7	30.4

for facilitating the lithium-ion transfer throughout the electrode. Graphite@NMC111/MWCNTs full cell shows lower lithium-ion diffusion coefficient than NMC111/MWCNTs half cell, because of SEI layer (solid electrolyte interphase) in between electrolyte and graphite anode [22].

4 Conclusions

In this paper, NMC111 powders with nanodimensions and high purity are successfully synthesized by the sol–gel method. NMC111/MWCNTs free-standing hybrid electrodes that are prepared by a vacuum filtration method without encroaching on the morphology and crystal structure of raw NMC111. By the method, NMC111 nanoparticles are decorated homogeneously between the highly conductive MWCNTs. MWCNTs not only present the electrode with a higher electrical conductivity but also effectively increase the cyclic stability of the cathode electrode compared to pure NMC111. After 1000 cycles at a 1 C rate, the specific discharge capacity of NMC111/MWCNTs free-standing hybrid electrode is 118.5 mAh g^{-1}, improved by

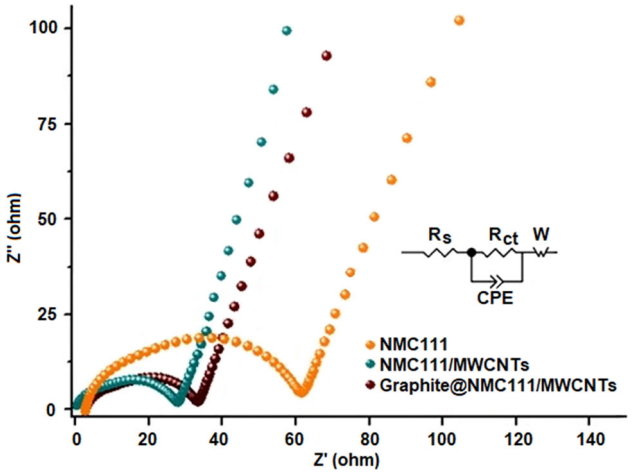

Fig. 7 Nyquist curve of the NMC111 electrode and NMC111/MWCNTs freestanding hybrid electrodes

Table 3 Resistance values and diffusion coefficients of NMC111, NMC111/MWCNTs, and graphite@NMC111/MWCNTs after cell assembly

Sample	R_s (Ω)	R_{ct} (Ω)	D_{Li}^+
NMC111	3.1	61	1.72×10^{-10}
NMC111/MWCNTs	1.0	29	5.06×10^{-11}
Graphite@NMC111/MWCNTs	2.9	37	7.57×10^{-11}

39% than pure NMC111 electrode (84.9 mAh g^{-1}). Electrochemical impedance spectroscopy has shown that the charge resistance of cathode electrodes reduces by MWCNTs reinforcement. Graphite@NMC111/MWCNTs full-cell was produced after the advanced electrochemical performance of NMC111/MWCNTs half-cell tests. In the full cells, NMC111 and MWCNTs-based freestanding electrode type supplied a discharge capacity of 150.7 mAh g^{-1} after 1000 cycles, certifying that this electrode type could improve the total battery performance.

Funding This study was funded by Sakarya University of Applied Sciences.

References

1. Nasir, F.M.; Abdullah, M.Z.; Ismail, M.A.: Experimental investigation of water-cooled heat pipes in the thermal management of lithium-ion EV batteries. Arab. J. Sci. Eng. **44**(9), 7541–7552 (2019). https://doi.org/10.1007/s13369-019-03851-5
2. Gröger, O.; Gasteiger, H.A.; Suchsland, J.-P.: Review—electromobility: batteries or fuel cells? J. Electrochem. Soc. **162**(14), A2605–A2622 (2015). https://doi.org/10.1149/2.0211514jes
3. Zhang, L.; Guo, J.: Understanding the reaction mechanism of lithium-sulfur batteries by in situ/operando X-ray absorption spectroscopy. Arab. J. Sci. Eng. **44**(7), 6217–6229 (2019). https://doi.org/10.1007/s13369-019-03808-8
4. Gallagher, K.G.; Goebel, S.; Greszler, T.; Mathias, M.; Oelerich, W.; Eroglu, D.; Srinivasan, V.: Quantifying the promise of lithium-air batteries for electric vehicles. Energy Environ. Sci. **7**(5), 1555–1563 (2014). https://doi.org/10.1039/c3ee43870h
5. Shaju, K.M.; Bruce, P.G.: Macroporous $LiNi_{1/3}Mn_{1/3}Co_{1/3}O_2$: a high-rate positive electrode for rechargeable lithium batteries. J. Power Sources **174**(2), 1201–1205 (2007). https://doi.org/10.1016/j.jpowsour.2007.06.091
6. Cao, X.; Zhao, Y.; Zhu, L.; Xie, L.; Cao, X.; Xiong, S., Wang, C.: Synthesis and characterization of $LiNi_{1/3}Mn_{1/3}Co_{1/3}O_2$ as cathode materials for Li-ıon batteries via an efficacious sol–gel method. Int. J. Electrochem. Sci. **11**(6), 5267–5278. https://doi.org/10.20964/2016.06.93.
7. Hashem, A.M.; Abdel-Ghany, A.E.; Abuzeid, H.M.; Ehrenberg, H.; Mauger, A.; Groult, H.; Julien, C.M.: $LiNi_{1/3}Mn_{1/3}Co_{1/3}O_2$ synthesized by sol–gel method: structure and electrochemical properties. ECS Trans. **50**(24), 91–96 (2013). https://doi.org/10.1149/05024.0091ecst
8. Vallverdu, G.; Minvielle, M.; Andreu, N.; Gonbeau, D.; Baraille, I.: First principle study of the surface reactivity of layered lithium oxides $LiMO_2$ (M = Ni, Mn, Co). Surf. Sci. **649**, 46–55 (2016). https://doi.org/10.1016/j.susc.2016.01.004
9. Seteni, B.; Rapulenyane, N.; Ngila, J. C.; Luo, H.: Structural and electrochemical behavior of $Li_{1.2}Mn_{0.54}Ni_{0.13}Co_{0.13-x}Al_xO_2$ (x = 0.05) positive electrode material for lithium ıon battery. Mater. Today Proc. **5**(4), 10479–10487 (2018). https://doi.org/10.1016/j.matpr.2017.12.379
10. Kim, G.-H.; Kim, J.-H.; Myung, S.-T.; Yoon, C.S.; Sun, Y.-K.: Improvement of high-voltage cycling behavior of surface-modified $LiNi_{1/3}Mn_{1/3}Co_{1/3}O_2$ cathodes by fluorine substitution for Li-ion batteries. J. Electrochem. Soc. **152**(9), A1707 (2005). https://doi.org/10.1149/1.1952747
11. Buchberger, I.; Seidlmayer, S.; Pokharel, A.; Piana, M.; Hattendorff, J.; Kudejova, P.; Gilles, R.; Gasteiger, H.A.: Aging analysis of graphite/$LiNi_{1/3}Mn_{1/3}Co_{1/3}O_2$ Cells Using XRD, PGAA, and AC impedance. J. Electrochem. Soc. **162**(14), A2737–A2746 (2015). https://doi.org/10.1149/2.0721514jes
12. Kim, S.J.; Lee, A.Y.; Park, H.C.; Kim, S.Y.; Kim, M.C.; Lee, J.M.; Kim, S.B.; Kim, W.S.; Jeong, Y.; Park, K.W.: carbon nanotube web-based current collectors for high-performance lithium ion batteries. Mater. Today Commun. **4**, 149–155 (2015). https://doi.org/10.1016/j.mtcomm.2015.06.010
13. Stiaszny, B.; Ziegler, J.C.; Krauß, E.E.; Zhang, M.; Schmidt, J.P.; Ivers-Tiffée, E.: Electrochemical characterization and post-mortem analysis of aged $LiMn_2O_4$-NMC/graphite lithium ion batteries part II: calendar aging. J. Power Sources **258**, 61–75 (2014). https://doi.org/10.1016/j.jpowsour.2014.02.019
14. Prompun, P.; Ratchahat, S.; Kaveevivitchai, W.; Kooamornpattana, W.: Carbon nanotube (CNTs) production from waste cooking oil as anode material for Li-ion batteries. J. Phys. Conf. Ser. **2175**(1), 012041 (2022). https://doi.org/10.1088/1742-6596/2175/1/012041
15. Guoping, W.; Qingtang, Z.; Zuolong, Y.; MeiZheng, Q.: The effect of different kinds of nano-carbon conductive additives in lithium ion batteries on the resistance and electrochemical behavior of the $LiCoO_2$ composite cathodes. Solid State Ionics **179**(7–8), 263–268 (2008). https://doi.org/10.1016/j.ssi.2008.01.015
16. Umar, Ahmad; Ahmed, Faheem; Ibrahim, Ahmed A.; Algadi, Hassan; Albargi, Hasan B.; Alhmami, Mohsen Ali M.; Almas, Tubia; Mohammed, Ayeda Y. A.; Abuhimd, Hatem; Castañeda, L. (2021). MnO_2 nanoparticles anchored multi walled carbon nanotubes as potential anode materials for lithium ıon batteries.

J. Nanosci. Nanotechnol. **21**(10), 5296–5301. https://doi.org/10.1166/jnn.2021.19440.
17. Du, Z.; Li, J.; Wood, M.; Mao, C.; Daniel, C.; Wood, D.L.: Three-dimensional conductive network formed by carbon nanotubes in aqueous processed NMC electrode. Electrochim. Acta **270**, 54–61 (2018). https://doi.org/10.1016/j.electacta.2018.03.063
18. Pan, C. Chi; Zhu, Y. Rong; Yang, Y. Chang; Hou, H. Shuai; Jing, M. Jun; Song, W. Xin; Yang, X. Ming; Ji, X. Bo: Influences of transition metal on structural and electrochemical properties of $Li[Ni_xCo_yMn_z]O_2$ ($0.6 \leq x \leq 0.8$) cathode materials for lithium-ıon batteries. Trans. Nonferrous Met. Soc. China (English Ed.) **26**(5), 1396–1402 (2016). https://doi.org/10.1016/S1003-6326(16)64244-9
19. Youn, D.Y.; Kim, C.; Cheong, J.Y.; Cho, S.H.; Yoon, K.R.; Jung, J.W.; Kim, N.H.; Kim, I.D.: Stable and high-capacity Si electrodes with free-standing architecture for lithium-ion batteries. ACS Appl. Energy Mater. **3**(1), 208–217 (2020). https://doi.org/10.1021/acsaem.9b01274
20. Spencer, M.A.; Augustyn, V.: Free-standing transition metal oxide electrode architectures for electrochemical energy storage. J. Mater. Sci. **54**(20), 13045–13069 (2019). https://doi.org/10.1007/s10853-019-03823-y
21. Abouimrane, A.; Ding, J.; Davidson, I.J.: Liquid electrolyte based on lithium bis-fluorosulfonyl imide salt: aluminum corrosion studies and lithium ion battery investigations. J. Power Sources **189**(1), 693–696 (2009). https://doi.org/10.1016/j.jpowsour.2008.08.077
22. Guler, A.; Gungor, H.; Ozcan, S.; Coban, A.; Guler, M.O.; Akbulut, H.: A high-performance composite positive electrode based on graphene and $Li(Ni_{1/3}\ Co_{1/3}Mn1_{/3})O_2$. Int. J. Energy Res. **42**(14), 4499–4511 (2018). https://doi.org/10.1002/er.4198
23. Nisa, S.S.; Rahmawati, M.; Yudha, C.S.; Nilasary, H.; Nursukatmo, H.; Oktaviano, H.S.; Purwanto, A.: A fast approach to obtain layered transition-metal cathode material for rechargeable batteries. Batteries **8**(1), 4 (2022). https://doi.org/10.3390/batteries8010004
24. Li, X.; Zhao, X.; Wang, M.S.; Zhang, K.J.; Huang, Y.; Qu, M.Z.; Zheng, J.M.: Improved rate capability of a LiNi1/3Co1/3Mn1/3O2/CNT/graphene hybrid material for Li-ion batteries. RSC Adv. **7**(39), 24359–24367 (2017). https://doi.org/10.1039/c7ra03438e
25. Yoon, S.; Jung, K. N.; Yeon, S. H.; Jin, C. S.; Shin, K. H. Electrochemical properties of $LiNi_{0.8}Co_{0.15}Al_{0.05}O_2$-graphene composite as cathode materials for lithium-ıon batteries. J. Electroanal. Chem. **683**, 88–93 (2012). https://doi.org/10.1016/j.jelechem.2012.08.005
26. Serpone, N.; Lawless, D.; Khairutdinov, R.: Size effects on the photophysical properties of colloidal anatase TiO_2 particles: size quantization or direct transitions in this indirect semiconductor? J. Phys. Chem. **99**(45), 16646–16654 (1995). https://doi.org/10.1021/j100045a026
27. Hu, G.; Liu, W.; Peng, Z.; Dua, K.; Cao, Y. Synthesis and electrochemical properties of $LiNi_{0.8}Co_{0.15}Al_{0.05}O_2$ prepared from the precursor $Ni_{0.8}Co_{0.15}Al_{0.05}OOH$. J. Power Sources **198**, 258–263 (2012). https://doi.org/10.1016/j.jpowsour.2011.09.101
28. Julien, C. M.; Mauger, A.; Trottier, J.; Zaghib, K.; Hovington, P.; Groult, H. Olivine-based blended compounds as positive electrodes for lithium batteries. Inorganics **4**(2) (2016). https://doi.org/10.3390/inorganics4020017.
29. Hwang, B.J.; Tsai, Y.W.; Chen, C.H.; Santhanam, R.: Influence of Mn content on the morphology and electrochemical performance of $LiNi_{1-x-y}Co_xMn_yO_2$ cathode materials. J. Mater. Chem. **13**(8), 1962–1968 (2003). https://doi.org/10.1039/b301468c
30. Zhang, L.; Fu, J.; Zhang, C. Mechanical composite of $LiNi_{0.8}Co_{0.15}Al_{0.05}O_2$/carbon nanotubes with enhanced electrochemical performance for lithium-ıon batteries. Nanoscale Res. Lett. (2017). https://doi.org/10.1186/s11671-017-2143-4
31. Luo, W.; Liu, L.; Li, X.; Yu, J.; Fang, C. Templated assembly of $LiNi_{0.8}Co_{0.15}Al_{0.05}O_2$/graphene nano composite with high rate capability and long-term cyclability for lithium ıon battery. J. Alloys Compd. **810**, 151786 (2019). https://doi.org/10.1016/j.jallcom.2019.151786
32. Mentbayeva, A.; Belgibayeva, A.; Umirov, N.; Zhang, Y.; Taniguchi, I.; Kurmanbayeva, I.; Bakenov, Z.: High performance freestanding composite cathode for lithium-sulfur batteries. Electrochim. Acta **217**, 242–248 (2016). https://doi.org/10.1016/j.electacta.2016.09.082
33. Yudha, C.S.; Muzayanha, S.U.; Widiyandari, H.; Iskandar, F.; Sutopo, W.; Purwanto, A. Synthesis of $LiNi_{0.85}Co_{0.14}Al_{0.01}O_2$ cathode material and ıts performance in an NCA/graphite full-battery. Energies **12**, 1886 (2019). https://doi.org/10.3390/en12101886
34. Gupta, H.; Singh, S.K.; Singh, V.K.; Tripathi, A.K.; Srivastava, N.; Tiwari, R.K.; Mishra, R.; Meghnani, D.; Singh, R.K.: Development of polymer electrolyte and cathode material for Li-batteries. J. Electrochem. Soc. **166**(3), A5187–A5192 (2019). https://doi.org/10.1149/2.0331903jes
35. Shaju, K.M.; Subba Rao, G.V.; Chowdari, B.V.R.: Performance of layered $Li(Ni_{1/3}Co_{1/3}Mn_{1/3})O_2$ as cathode for Li-ion batteries. Electrochim. Acta **48**(2), 145–151 (2002). https://doi.org/10.1016/S0013-4686(02)00593-5
36. Qin, G.; Wu, Q.; Zhao, J.; Ma, Q.; Wang, C.: C/$LiFePO_4$/multi-walled carbon nanotube cathode material with enhanced electrochemical performance for lithium-ion batteries. J. Power Sources **248**, 588–595 (2014). https://doi.org/10.1016/j.jpowsour.2013.06.070
37. Kim, D.W.; Zettsu, N.; Teshima, K.: Three-dimensional SWCNT and MWCNT hybrid networks for extremely high-loading and high rate cathode materials. J. Mater. Chem. A **7**(29), 17412–17419 (2019). https://doi.org/10.1039/c9ta03870a
38. Wagner, N.P.; Asheim, K.; Vullum-Bruer, F.; Svensson, A.M. Performance and failure analysis of full cell lithium ıon battery with $LiNi_{0.80}Co_{0.15}Al_{0.05}O_2$ and silicon electrodes. J. Power Sources **437**, 226884 (2019). https://doi.org/10.1016/j.jpowsour.2019.226884
39. Song, C.; Wang, W.; Peng, H.; Wang, Y.; Zhao, C.; Zhang, H.; Tang, Q.; Lv, J.; Du, X.; Dou, Y.: Improving the electrochemical performance of $LiNi_{0.80}Co_{0.15}Al_{0.05}O_2$ in lithium ıon batteries by $LiAlO_2$ surface modification. Appl. Sci. (2018). https://doi.org/10.3390/app8030378
40. Wu, F.; Yan, Y.; Wang, R.; Cai, H.; Tong, W.; Tang, H.: Synthesis of $LiCo_{1/3}Ni_{1/3}Mn_{1/3}O_2$ @graphene for lithium-ion batteries via self-assembled polyelectrolyte layers. Ceram. Int. **43**(10), 7668–7673 (2017). https://doi.org/10.1016/j.ceramint.2017.03.066
41. Ivanishchev, A.V.; Churikov, A.V.; Ivanishcheva, I.A.; Ushakov, A.V.: Lithium diffusion in $Li_3V_2(PO_4)_3$-based electrodes: a joint analysis of electrochemical impedance, cyclic voltammetry, pulse chronoamperometry, and chronopotentiometry data. Ionics (Kiel). **22**(4), 483–501 (2016). https://doi.org/10.1007/s11581-015-1568-y
42. Huang, Z.D.; Liu, X.M.; Oh, S.W.; Zhang, B.; Ma, P.C.; Kim, J.K.: Microscopically porous, interconnected single crystal $LiCo_{1/3}Ni_{1/3}Mn_{1/3}O_2$ cathode material for lithium ion batteries. J. Mater. Chem. **21**(29), 10777–10784 (2011). https://doi.org/10.1039/c1jm00059d
43. He, J.R.; Chen, Y.F.; Li, P.J.; Wang, Z.G.; Qi, F.; Liu, J.B.: Synthesis and electrochemical properties of graphene-modified $LiCo_{1/3}Ni_{1/3}Mn_{1/3}O_2$ cathodes for lithium ion batteries. RSC Adv. **4**(5), 2568–2572 (2014). https://doi.org/10.1039/c3ra45115a